

MOLECULAR OUTFLOWS IN THE SUBSTELLAR DOMAIN: MILLIMETER OBSERVATIONS OF YOUNG VERY LOW MASS OBJECTS IN TAURUS AND ρ OPHIUCHI

NGOC PHAN-BAO,^{1,2} CHIN-FEI LEE,² PAUL T.P. HO,^{2,3} YA-WEN TANG²

Draft version March 4, 2022

ABSTRACT

We report here our search for molecular outflows from young very low mass stars and brown dwarfs in Taurus and ρ Ophiuchi. Using the Submillimeter Array (SMA) and the Combined Array for Research in Millimeter-wave Astronomy (CARMA), we have observed 4 targets at 1.3 mm wavelength (230 GHz) to search for CO J=2→1 outflows. A young very low mass star MHO 5 (in Taurus) with an estimated mass of 90 M_J , which is just above the hydrogen-burning limit, shows two gas lobes that are likely outflows. While the CO map of MHO 5 does not show a clear structure of outflow, possibly due to environment gas, its position-velocity diagram indicates two distinct blue- and redshifted components. We therefore conclude that they are components of a bipolar molecular outflow from MHO 5. We estimate an outflow mass of $7.0 \times 10^{-5} M_\odot$ and a mass-loss rate of $9.0 \times 10^{-10} M_\odot$. These values are over two orders of magnitude smaller than the typical ones for T Tauri stars and somewhat weaker than those we have observed in the young brown dwarf ISO-Oph 102 of 60 M_J in ρ Ophiuchi. This makes MHO 5 the first young very low mass star showing a bipolar molecular outflow in Taurus. The detection boosts the scenario that very low mass objects form like low-mass stars but in a version scaled down by a factor of over 100.

Subject headings: ISM: jets and outflows — ISM: individual ([BHS98] MHO 5, [GY92] 3, ISO-Oph 32, 2MASS J04390396+2544264, 2MASS J04414825+2534304) — stars: formation — stars: low mass, brown dwarfs — technique: interferometric

1. INTRODUCTION

Stars with a few solar masses can form by direct gravitational collapse mechanism (e.g., Shu et al. 1987). The typical process of star formation starts with collapse, accretion and launching of material as a bipolar outflow (Lada 1985). For the case of very low mass objects at the bottom of the main sequence, brown dwarfs (BD) (15–75 M_J) and very low-mass (VLM) stars (0.1–0.2 M_\odot) have masses significantly below the typical Jeans mass ($\sim 1 M_\odot$) in molecular clouds, and hence it is difficult to make a VLM stellar embryo by direct gravitational collapse but prevent subsequent accretion of material onto the central object once the VLM embryo formed. These VLM objects are therefore thought to form by different mechanisms (see Whitworth et al. 2007 and references therein). Two major models have been proposed for their formation. In the standard formation model, they form like low-mass stars just in a scaled-down version, through gravitational collapse and turbulent fragmentation of low-mass cores (e.g., Padoan & Nordlund 2004). In the ejection scenario, the VLM objects are simply stellar embryos ejected from unstable multiple protostellar systems by dynamical interaction with the other embryos. These VLM embryos are ejected from their gas reservoir and then they become VLM stars and BDs (e.g., Reipurth & Clarke 2001; Bate et al. 2002;

Bate & Bonnell 2005).

Observations (see Luhman et al. 2007 and references therein) of the BD and VLM star properties in different star-forming regions such as their initial mass function, velocity and spatial distributions, multiplicity, accretion disks and jets have demonstrated that stars and BDs share similar properties. This strongly supports the scenario that BDs and VLM stars form as low-mass stars do. One should note that additional mechanisms (e.g., the ejection) are possible but they are not likely dominant in making VLM objects.

More observations are needed to understand how these VLM objects form, especially observations at very early stages provide us an insight into the VLM object formation mechanism. Phan-Bao et al. (2008) reported the first detection of a bipolar molecular outflow from the young BD ISO-Oph 102 ($\sim 60 M_J$) in the ρ Ophiuchi dark cloud. The outflow mass and the mass loss rate are over 2 orders of magnitude smaller than the typical values detected for T Tauri stars. Their result demonstrates that the molecular outflow process occurs in BDs as a scaled-down version of that seen in low-mass stars. As the molecular outflow is a fundamental part of the star formation process, the detection of molecular outflows in VLM stars and BDs therefore extends our understanding of star formation in the lowest mass domain.

Up to date, there are only two molecular outflows detected in the substellar domain: from L1014-IRS, a possible proto-BD (Bourke et al. 2005; Huard et al. 2006) and ISO-Oph 102, a young BD (Phan-Bao et al. 2008). In this paper, we present our millimeter observations of 3 BDs and 1 VLM star in Taurus and ρ Ophiuchi. We detected a bipolar molecular outflow from the young VLM star MHO 5 whose outflow properties are similar to those

¹ Department of Physics, HCMIU, Vietnam National University Administrative Building, Block 6, Linh Trung Ward, Thu Duc District, HCM, Vietnam; pnbngoc@hcmiu.edu.vn

² Institute of Astronomy and Astrophysics, Academia Sinica, P.O. Box 23-141, Taipei 106, Taiwan, ROC; pbnngoc@asiaa.sinica.edu.tw

³ Harvard-Smithsonian Center for Astrophysics, Cambridge, MA

we observed in ISO-Oph 102.

Sec. 2 presents our sample, Sec. 3 reports our millimeter observations and the data reduction, Sec. 4 discusses outflow properties observed in MHO 5 and Sec. 5 summarizes our results.

2. SAMPLE SELECTION

Following the discovery of a bipolar molecular outflow in ISO-Oph 102, we selected 4 additional targets in ρ Ophiuchi and Taurus (see Table 1). They were selected from the lists of VLM accretors given in Muzerolle et al. (2003, 2005) for Taurus and Natta et al. (2004) for ρ Ophiuchi to cover a wide range of mass from 35 to 90 M_J , one of them (MHO 5) is a very low-mass star. These sources are the strongest accretors for a given mass. In addition, the detection of signatures of outflows from the literature was also considered to select the sources. Two of them MHO 5 and ISO-Oph 32 show forbidden emission lines (FELs) that could be associated with outflow activities. The detection of the blueshifted jet component of ISO-Oph 32 has been reported in Whelan et al. (2009). They are therefore good targets for our molecular outflow search.

3. OBSERVATIONS AND DATA REDUCTION

We observed 4 VLM objects in Taurus and ρ Ophiuchi with SMA and CARMA. The observing log is given in Table 1.

3.1. SMA observations

Observations of MHO 5 and ISO-Oph 32 were carried out with the receiver band at 230 GHz of the SMA⁴ (Ho et al. 2004) on November 16th 2008 and June 8th 2009, respectively. Zenith opacities at 225 GHz were typically in the range 0.15–0.2 and 0.05–0.1 for MHO 5 and ISO-Oph 32, respectively. Both 2 GHz-wide sidebands, which are separated by 10 GHz, were used. The SMA correlator was configured with high spectral resolution bands of 512 channels per chunk of 104 MHz for ¹²CO, ¹³CO, and C¹⁸O $J = 2 \rightarrow 1$ lines, giving a channel spacing of 0.27 km s⁻¹. A lower resolution of 3.25 MHz per channel was set up for the remainder of each sideband. The quasars 0428+329, 0510+180 and 3C 454.3 have been observed for gain and passband calibration of MHO 5, respectively. In the case of ISO-Oph 32, the quasars 1625–254 and 3C 273 were used. Uranus was used for flux calibration for both the targets. The uncertainty in the absolute flux calibration is about 10%. The data were calibrated using the MIR software package and further analysis was carried out with the MIRIAD package adapted for the SMA. All 8 antennas were operated in the compact configuration, resulting in synthesized beams of 3''.05 \times 2''.82 and 3''.78 \times 3''.38 using natural weighting for MHO 5 and ISO-Oph 32, respectively. The primary FWHM beam is about 50'' at the observed frequencies. The rms sensitivity was about 1 mJy for the continuum, using both sidebands and \sim 0.2 Jy beam⁻¹ per channel for the line data. We did not detect the dust continuum emission with an upper limit of 3 mJy measured at the VLM star position.

⁴ The Submillimeter Array is a joint project between the Smithsonian Astrophysical Observatory and the Academia Sinica Institute of Astronomy and Astrophysics and is funded by the Smithsonian Institution and the Academia Sinica.

3.2. CARMA observations

The two least massive BDs 2M 0439 and 2M 0441 in our sample were observed with CARMA in February and March 2009. All six 10.4-meter, nine 6.1-meter antennas were operated in the D configuration (a beam size of 2.4'' \times 2.0'') at 230 GHz. Zenith opacities at 227 GHz were typically in the range 0.3–0.4 and 0.2–0.3 for 2M 0439 and 2M 0441, respectively. As CARMA with a larger collecting area is more sensitive than SMA, the array is therefore suitable for our outflow search in these BDs. In semester 2009A, all three 500 MHz-wide bands (1.5 GHz maximum bandwidth per sideband), which may be positioned independently with the IF bandwidth, were used for CO search with different spectral resolutions. For our observations, three bands were configured in the following modes: 8 MHz and 31 MHz with 63 channels per band, and 500 MHz with 15 channels per band, resulting in spectral resolutions of 0.17, 0.64, and 43.4 km s⁻¹, respectively. The quasar 3C 111 has been observed for gain, and 3C 84 for passband and flux calibration. The uncertainty in the absolute flux calibration is about 10%. The data were reduced with the MIRIAD package adapted for the CARMA. The synthesized beam sizes are about 2''.60 \times 2''.48 and 2''.02 \times 1''.86 (natural weighting) for 2M 0439 and 2M 0441, respectively. The primary FWHM beam is about 36'' at 230 GHz. For the continuum, the rms sensitivity was about 0.4 mJy. For the line data, the sensitivities are 0.1 and 0.05 Jy beam⁻¹ per channel for 8 and 31 MHz band, respectively.

4. DISCUSSION

4.1. 2M 0439 and 2M 0441

Two young BDs in Taurus 2MASS J04390396+2544264 (M7.25, 50 M_J , Luhman 2004; Muzerolle et al. 2005) and 2MASS J04414825+2534304 (M7.75, 35 M_J , Luhman 2004; Muzerolle et al. 2005) are strong accretors with an estimated accretion rate $\log M_{\text{acc}}(M_{\odot} \text{ yr}^{-1}) = -11.3$ for both the BDs (Muzerolle et al. 2005). These BDs are included in our sample with an aim of probing molecular outflows for the lowest mass BDs. Up to date, no outflow signatures from these two BDs have been reported.

The dust continuum fluxes are 2.4 \pm 0.4 mJy and 2.2 \pm 0.4 mJy measured at the position of 2M 0439 and 2M 0441, respectively. Our measurements are consistent with the previous ones (Scholz et al. 2006).

Our CO maps from CARMA data do not reveal any outflow. The non-detection of outflows indicates three possibilities: (1) the outflow process in these BDs itself is too weak to produce detectable outflows; (2) this process has already stopped; (3) there is not enough environment gas around the sources to produce detectable outflows. Guieu et al. (2007) reported the presence of an inner hole in these BD disks (see table 4), indicating these BDs in the transitional stage between class II and III objects, which are at later stages than that of embedded proto-BD candidates such as L1014-IRS (class I, Bourke et al. 2005) or SSTB213 J041757 (class I, Barrado et al. 2009). This therefore supports the second scenario. However one should note that the outflow process in BDs might last longer than that in low-mass stars as seen in ISO-Oph 102 (Phan-Bao et al. 2008). Therefore the first scenario can not be ruled out.

4.2. ISO-Oph 32

ISO-Oph 32 (or [GY9] 3) is an M7.5 accreting BD (class II) with an estimated mass of 40 M_J and an accretion rate $\log \dot{M}_{\text{acc}}(M_{\odot} \text{ yr}^{-1}) = -10.5$ estimated from H α profiles (Natta et al. 2004). The dust continuum is not detected and we obtain an upper limit of 1.0 mJy at the BD position.

Whelan et al. (2009) reported the detection of a weak jet in this BD from the [OI] 6300Å line at a signal-to-noise ratio of just above 4. However, the CO map of ISO-Oph 32 based on our SMA observations does not show any outflow, possibly due to either the molecular outflow process is too weak to be detectable with our current sensitivity or surrounding gas is not dense enough to produce detectable molecular outflows. Deeper observations are required to confirm the previous detection of a jet and to characterize the molecular outflow from this BD.

4.3. MHO 5

MHO 5, a young (~ 1 – 2 Myr) M6 dwarf initially identified by Briceño et al. (1998), is located in the Taurus dark cloud at a distance of 147 parsecs (Loinard et al. 2007). Briceño et al. (1998) (see also Muzerolle et al. 2003) detected forbidden [OI] emission lines at 6300 and 6364 Å. Such forbidden emission lines are typically associated with accretion disks or outflows (Alencar et al. 2005; Hartigan et al. 1995). The estimated mass is 90 M_J (Muzerolle et al. 2003), which is just above the hydrogen-burning limit. The optical visibility of MHO 5 suggests that the source corresponds to a class II object (Lada 1985) in the star formation phase, a class with an accreting circumstellar disk and the protostar at this stage is the so-called classical T Tauri star.

Figure 1 presents an overlay of a near-infrared image and the integrated intensity in the carbon monoxide (CO $J = 2 - 1$) line emission. Two blue- and redshifted CO lobes are detected around the position of the central object. Both lobes show elongated structures and but they are not symmetrically displaced on opposite sides of the MHO 5 position as was seen in ISO-Oph 102. However the position-velocity (P-V) diagram for the CO emission cut at a position angle of 62° clearly indicates two blue- and redshifted components (Fig. 2). The elongated structures are probably due to a mixture of outflows from MHO 5 and nearby massive outflows from class 0 and I protostars in the L1551 molecular cloud, a multigenerational star formation region (see Moriarty-Schieven et al. 2006). Based on the P-V diagram and assuming that the MHO 5 outflow components are symmetric, we consider the outflow from MHO 5 to consist of only the blueshifted component with the peak at velocity ~ 3 km s $^{-1}$ and the redshifted component with the peak at velocity ~ 5 km s $^{-1}$ as indicated Fig. 2. The CO gas velocity at the source position is 4.2 km s $^{-1}$ and our spectral resolution is 0.27 km s $^{-1}$, we therefore estimate the systemic velocity of MHO 5 to be about 4.2 ± 0.3 km s $^{-1}$. This value is in good agreement with a velocity of 4.0 km s $^{-1}$, which is determined by taking an average of the velocities of red- and blueshifted components as used to determine the systemic velocity of ISO-Oph 102 (Phan-Bao et al. 2008). One should note that these estimates suffer some uncertainties due to some problems such as missing flux,

outflow contamination for the first estimate or outflow morphology for the second one. More observations are needed to exactly determine the systemic velocity. If this systemic velocity is shifted by the uncertainty of 0.3 km s $^{-1}$ in either direction, the blueshifted and redshifted contours will not significantly change as the MHO 5 outflow shows two distinct outflow components in the velocity ranges 2.6–3.8 km s $^{-1}$ and 4.5–5.7 km s $^{-1}$, which are not affected by the shift of systemic velocity. One should note that the origin of extended redshifted components around 4.4 and 5.2 km s $^{-1}$ at an offset position of $\sim 8''$ and around 6.0 km s $^{-1}$ at a position of $\sim 6''$ (see Fig. 2) is not clear, we therefore do not include them in our outflow mass calculation. However, if these extended components are included in the MHO 5 outflow, its outflow mass will increase by a factor of ~ 2 . This increase in outflow mass however will not change our main conclusion on the outflow properties of MHO 5 comparing to those of low-mass stars.

We then measure the size of each lobe of about $4''$ corresponding to ~ 600 AU in length. The two outflow components likely show a bow-shock structure as seen in ISO-Oph 102, an effect of the interaction between the jet propagation and the ambient material (e.g., Lee et al. 2000; Masson & Chernin 1993). Following the standard manner (Cabrit & Bertout 1990; André et al. 1990) as used in the previous paper (Phan-Bao et al. 2008), we calculate the outflow properties. We use a value of 35 K (Loren et al. 1983) for the excitation temperature, and we derive a lower limit to the outflow mass $M_{\text{flow}} \sim 1.4 \times 10^{-5} M_{\odot}$. If we correct for optical depth with a typical value of 5 (Levreault 1988a), we obtain an upper limit to the outflow mass of $7.0 \times 10^{-5} M_{\odot}$. One should note that a missing flux factor for SMA is not applied for the upper limit. This value is smaller than the typical values 0.01–0.7 M_{\odot} of young low-mass stars (class II with G, K spectral types, see Levreault 1988b and references therein) by over three orders of magnitude.

We use the observed maximum flow velocity of 1.8 km s $^{-1}$ and apply a correction for an outflow inclination, which is derived from a disk inclination of $\sim 30^\circ$ (B. Riaz, private communication), to compute upper limit values for the kinematic and dynamic parameters. We find that the momentum is $P = 2.8 \times 10^{-5} M_{\odot} \text{ km s}^{-1}$, the energy is $E = 3.0 \times 10^{-5} M_{\odot} \text{ km}^2 \text{ s}^{-2}$, the force is $F = 1.8 \times 10^{-8} M_{\odot} \text{ km s}^{-1} \text{ yr}^{-1}$, and the mechanical luminosity is $L = 3.1 \times 10^{-6} L_{\odot}$, where L_{\odot} is the solar luminosity. A correction for the optical depth factor of 5 and a missing flux factor of 3 for SMA (Bourke et al. 2005) will increase these upper limit values by a factor of 15. Using the lower value of the outflow mass and a correction factor of 10 applied for the outflow duration time (Parker et al. 1991), we derive the outflow mass-loss rate $\dot{M}_{\text{out}} = 9.0 \times 10^{-10} M_{\odot} \text{ yr}^{-1}$, which is smaller than a typical value of $10^{-7} M_{\odot} \text{ yr}^{-1}$ for T Tauri stars (see Lada 1985) by two orders of magnitude. One should note that the correction factors were also applied in the same manner to calculate the outflow properties of ISO-Oph 102 (Phan-Bao et al. 2008). The outflow mass and the mass loss rate values from MHO 5 are somewhat weaker than that from ISO-Oph 102 but they are comparable to each other. This can be explained by a weaker activity of the jet in MHO 5 than in ISO-Oph

102, e.g., [SII] 6716 and 6731 Å only detected in ISO-Oph 102 (Briceño et al. 1998; Natta et al. 2004), and a lower gas density surrounding MHO 5 (Taurus) than in ISO-Oph 102 (ρ Ophiuchi) (see Tachihara et al. 2000). One should note that the outflow of these sources share similar outflow mass and mass loss rate with the proto-BD candidate L1014-IRS, $M_{\text{flow}} \sim 1.4 \times 10^{-5} M_{\odot}$ and $\dot{M}_{\text{out}} = 2 \times 10^{-9} M_{\odot} \text{ yr}^{-1}$ (Bourke et al. 2005). The accretion and mass loss rates for these sources are listed in Table 2.

We also examine the possibility that the emission might be due to bound motions and not outflow emission. This would require an enclosed mass of $1.1 M_{\odot}$ for an outflow size of 600 AU with a velocity of 1.8 km s^{-1} , which is significantly larger than the core mass of $< 0.2 M_{\odot}$ within the same radius (Onishi et al. 2002). We therefore conclude that the detected emission is from the outflow.

We also reduced and analyzed infrared observations of MHO 5, 2M 0439, and 2M 0441 from the Spitzer Space Telescope's archival data. The IRS infrared (SL: 5.2-14.5 μm ; LL: 14.0-38.0 μm) (Houck et al. 2004) spectra of the three sources, were produced from the basic-calibrated data downloaded from the Spitzer archive (PID: 30540, 2) and reduced using the SMART software package (Higdon et al. 2004). All their mid-infrared spectra (see Fig. 3) exhibit strong crystalline silicate features (enstatite at 9.3 μm and forsterite at 11.3 μm), which appear similar to that seen in ISO-Oph 102 (Phan-Bao et al. 2008) and other VLM stars and BDs (Apai et al. 2005; Merín et al. 2007; Riaz 2009). The strong exhibition of crystalline silicates provides a direct evidence of grain growth and dust settling in the VLM star and BD disk. In the case of MHO 5, the molecular outflow process, which sweeps out gas from the disk, coexisting with grain growth and crystallization may favor rocky planets forming around this VLM star. One should note that this

coexistence phenomenon has also been observed in ISO-Oph 102.

5. SUMMARY

Here, we report our search for molecular outflows from VLM stars, BDs and the discovery of the bipolar molecular outflow in the young VLM star MHO 5. We point out that the bipolar molecular outflow in VLM stars is very similar to outflows as seen in young stars but scaled down by three and two orders of magnitude for the outflow mass and the mass-loss rate, respectively. This additional evidence strongly supports the scenario that VLM stars, BDs, and perhaps young planetary mass objects can launch a bipolar molecular outflow. If so, these objects may have a common origin with the low-mass stars. The detection of the coexistence phenomenon of molecular outflow, grain growth and crystallization processes in MHO 5 and ISO-Oph 102 provides an important implication for rocky planet search around VLM stars and BDs.

N.P.-B has been supported by VietNam NAFOSTED grant 103.08-2010.07. Support for CARMA construction was derived from the Gordon and Betty Moore Foundation, the Kenneth T. and Eileen L. Norris Foundation, the James S. McDonnell Foundation, the Associates of the California Institute of Technology, the University of Chicago, the states of California, Illinois, and Maryland, and the National Science Foundation. Ongoing CARMA development and operations are supported by the National Science Foundation under a cooperative agreement, and by the CARMA partner universities. This work is based in part on observations made with the Spitzer Space Telescope, which is operated by the Jet Propulsion Laboratory, California Institute of Technology, under a contract with NASA. This work has made use of the Centre de Données astronomiques de Strasbourg (CDS) database.

REFERENCES

- Alencar, S. H. P., Basri, G., Hartmann, L., & Calvet, N. 2005, *A&A*, 440, 595
- André, P., Martín-Pintado, J., Despois, D., & Montmerle, T. 1990, *A&A*, 236, 180
- Apai, D., Pascucci, I., Bouwman, J., Natta, A., Henning, T., & Dullemond, C. P. 2005, *Science*, 310, 834
- Barrado y Navascués, D., Mohanty, S., & Jayawardhana, R. 2004, *ApJ*, 604, 284
- Barrado, D., et al. 2009, *A&A*, 508, 859
- Bate, M. R., Bonnell, I. A., & Bromm, V. 2002, *MNRAS*, 332, L65
- Bate, M. R., & Bonnell, I. A. 2005, *MNRAS*, 356, 1201
- Briceño, C., Hartmann, L., Stauffer, J., & Martín, E. L. 1998, *AJ*, 115, 2074
- Bourke, T. L., Crapsi, A., Myers, P. C., Evans, Neal J., II, Wilner, D. J., Huard, T. L., Jørgensen, J. K., & Young, C. H. 2005, *ApJ*, 633, L129
- Cabrit, S., & Bertout, C. 1990, *ApJ*, 348, 530
- de Geus, E. J., de Zeeuw, P. T., & Lub, J. 1989, *A&A*, 216, 44
- Fernández, M., & Comerón, F. 2001, *A&A*, 380, 264
- Fernández, M., & Comerón, F. 2005, *A&A*, 440, 1119
- Greene, T.P., & Young, E. T. 1992, *ApJ*, 395, 516
- Guieu, S., et al. 2007, *A&A*, 465, 855
- Hartigan, P., Edwards, S., & Ghandour, L. 1995, *ApJ*, 452, 736
- Hauschildt, P. H., Allard, F., & Barron, E. 1999, *ApJ*, 512, 377
- Higdon, S. J. U., et al. 2004, *PASP*, 116, 975
- Ho, P. T. P., Moran, J. M., & Lo, K. Y. 2004, *ApJ*, 616, L1
- Houck, J. R., et al. 2004, *ApJS*, 154, 18
- Huard, T. L., et al. 2006, *ApJ*, 640, 391
- Lada, C. J. 1985, *ARA&A*, 23, 267
- Lee, C.-F., Mundy, L. G., Reipurth, B., Ostriker, E. C., & Stone, J. M. 2000, *ApJ*, 542, 925
- Levreault, R. M. 1988a, *ApJS*, 67, 283
- Levreault, R. M. 1988b, *ApJ*, 330, 897
- Loinard, L., Torres, R. M., Mioduszewski, A. J., Rodríguez, L. F., González-Lópezlira, R. A., Lachaume, R., Vázquez, V., & González, E. 2007, *ApJ*, 671, 546
- Loren, R. B., Sandqvist, A., & Wootten, A. 1983, *A&A*, 270, 620
- Luhman, K. L. 2004, *ApJ*, 617, 1216
- Luhman, K. L., Joergens, V., Lada, C., Muzerolle, J., Pascucci, I., & White, R. 2007, in *Protostars and Planets V*, ed. B. Reipurth, D. Jewitt, & K. Keil (Tucson: Univ. Arizona Press), 443
- Martín, E.L., Dougados, C., Magnier, E., Ménard, F., Magazzù, A., Cuillandre, J.-C., & Delfosse, X. 2001, *ApJ*, 561, L195
- Martín, E. L., Rebolo, R., & Magazzù, A. 1994, *ApJ*, 436, 262
- Masson, C. R., & Chernin, L. M. 1993, *ApJ*, 414, 230
- Merín, B., et al. 2007, *ApJ*, 661, 361
- Min, M., Hovenier, J. W., & de Koter, A. 2003, *A&A*, 404, 35
- Min, M., Hovenier, J. W., & de Koter, A. 2005, *A&A*, 432, 909
- Moriarty-Schieven, G. H., Johnstone, D., Bally, J., & Jenness, T. 2006, *ApJ*, 645, 357
- Muzerolle, J., Hillenbrand, L., Calvet, N., Briceño, C., & Hartmann, L. 2003, *ApJ*, 592, 266

- Muzerolle, J., Luhman, K. L., Briceño, C., Hartmann, L., & Calvet, N. 2005, *ApJ*, 625, 906
- Natta, A., Testi, L., Comerón, F., Oliva, E., D'Antona, F., Baffa, C., Comoretto, G., & Gennari, S. 2002, *A&A*, 393, 597
- Natta, A., Testi, L., Muzerolle, J., Randich, S., Comerón, F., & Persi, P. 2004, *A&A*, 424, 603
- Onishi, T., Mizuno, A., Kawamura, A., Ogawa, H., & Fukui, Y. 2002, *ApJ*, 575, 950
- Padoan, P., & Nordlund, Å. 2004, *ApJ*, 617, 559
- Parker, N. D., Padman, R., & Scott, P. F. 1991, *MNRAS*, 252, 442
- Phan-Bao, N., et al. 2008, *ApJ*, 689, L141
- Reipurth, B., & Clarke, C. J. 2001, *AJ*, 122, 432
- Riaz, B., & Gizis, J. E. 2008, *ApJ*, 681, 1584
- Riaz, B. 2009, *ApJ*, 701, 571
- Scholz, A., Jayawardhana, R., & Wood, K. 2006, *ApJ*, 645, 1498
- Shu, F. H., Adams, F. C., & Lizano, S. 1987, *ARA&A*, 25, 23
- Stassun, K. G., Mathieu, R. D., & Valenti, J. A. 2005, *Nature*, 440, 311
- Tachihara, K., Mizuno, A., & Fukui, Y. 2000, *ApJ*, 528, 817
- van Boekel, R., Waters, L. B. F. M., Dominik, C., Bouwman, J., de Koter, A., Dullemond, C. P., & Paresce, F. 2003, *A&A*, 400, L21
- Whelan, E. T., Ray, T. P., Bacciotti, F., Natta, A., Testi, L., Randich, S. 2005, *Nature*, 435, 652
- Whelan, E. T., Ray, T. P., Randich, S., Bacciotti, F., Jayawardhana, R., Testi, L., Natta, A., & Mohanty, S. 2007, *ApJ*, 659, L45
- Whelan, E. T., Ray, T. P., Podio, L., Bacciotti, F., & Randich, S. 2009, *ApJ*, 706, 1054
- Whitworth, A., Bate, M. R., Nordlund, Å., Reipurth, B., & Zinnecker, H. 2007, in *Protostars and Planets V*, ed. B. Reipurth, D. Jewitt, & K. Keil (Tucson: Univ. Arizona Press), 459

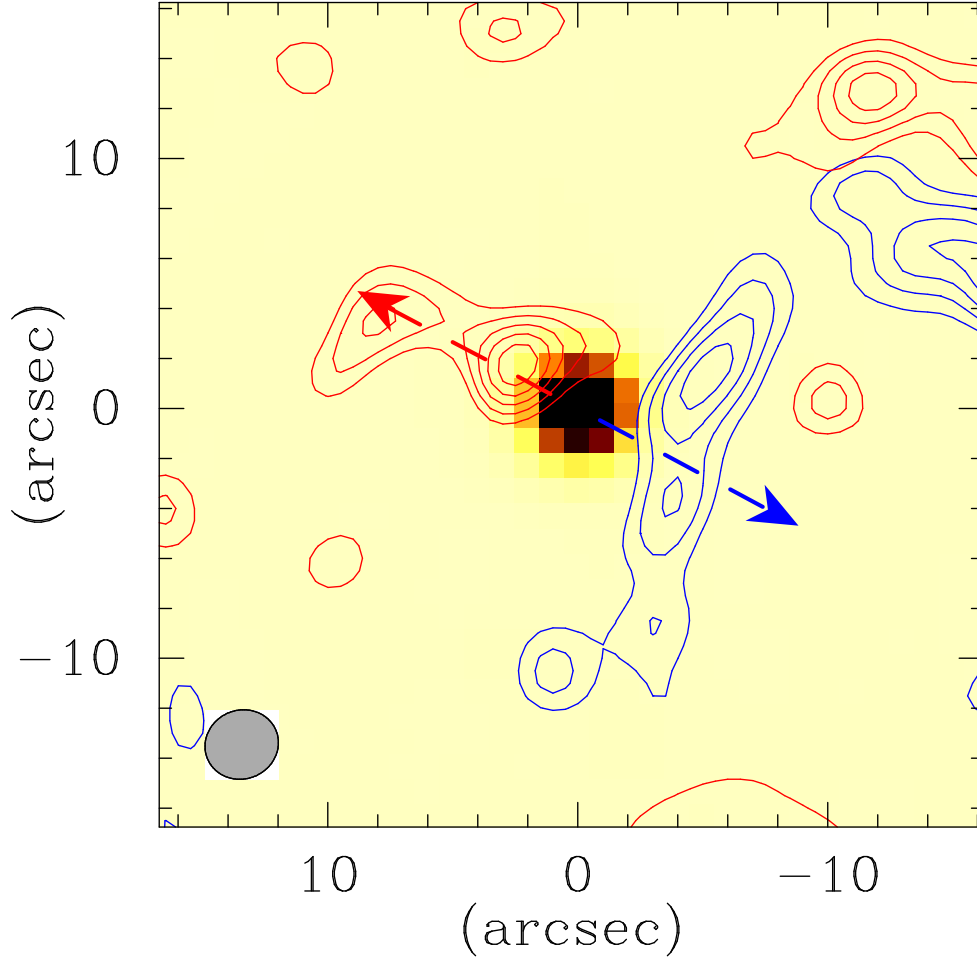


FIG. 1.— An overlay of the J-band ($1.25 \mu\text{m}$) near-infrared Two Micron All Sky Survey (2MASS) image and the integrated intensity in the carbon monoxide ($\text{CO } J = 2-1$) line emission from 2.45 to 6.15 km s^{-1} line-of-sight velocities. The blue and red contours represent the blueshifted (integrated over 2.45 and 3.77 km s^{-1}) and redshifted (integrated over 4.56 and 6.15 km s^{-1}) emissions, respectively. The contours are 4, 6, 8,...times the rms of $0.12 \text{ Jy beam}^{-1} \text{ km s}^{-1}$. The brown dwarf is visible in the J-band image. The position angle of the outflow is about 62° . The outflow directions are indicated by the blue and red arrows. The blue- and redshifted gas lobes are displaced on opposite sides of the brown dwarf center with an offset of about $2''$. An elongated structure is visibly seen in the blueshifted component while the redshifted one shows an extended component (see Sec. 4.3 for discussion). The gas lobes in the top right corner are expected to be outflows from nearby massive outflows in the L1551 molecular cloud (see Fig. 4 and Fig. 15 in Moriarty-Schieven et al. 2006). The synthesized beam is shown in the bottom left corner.

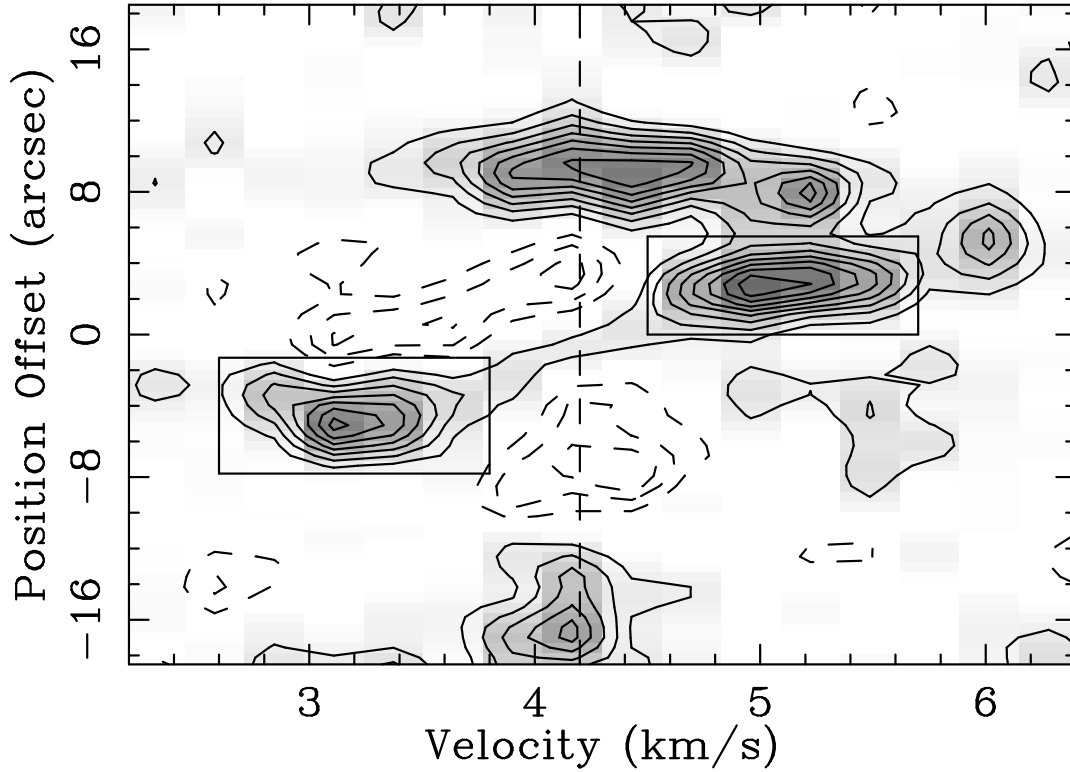


FIG. 2.— Position-Velocity (PV) cut diagram for CO $J = 2 \rightarrow 1$ emission at a position angle of 62° . The contours are $-8, -6, -4, -2, 2, 4, 6, 8, \dots$ times the rms of 0.1 Jy beam^{-1} . The blueshifted ($2.6\text{-}3.8 \text{ km s}^{-1}$) and redshifted ($4.5\text{-}5.7 \text{ km s}^{-1}$) components expected from MHO 5 are indicated by boxes, which we take to estimate the MHO 5 outflow properties (see Sec. 4.3 for discussion). The gas velocity at the source position is $4.2 \pm 0.3 \text{ km s}^{-1}$, which we take to be the systemic velocity of the VLM star as indicated by the dashed line. Both blue- and redshifted components shows a wide range of the velocity in their structure, which appears to be the bow-shock surfaces as observed in young stars (Lee et al. 2000). These surfaces are formed at the head of the jet and accelerate the material in the bow-shock sideways (e.g., Masson & Chernin 1993).

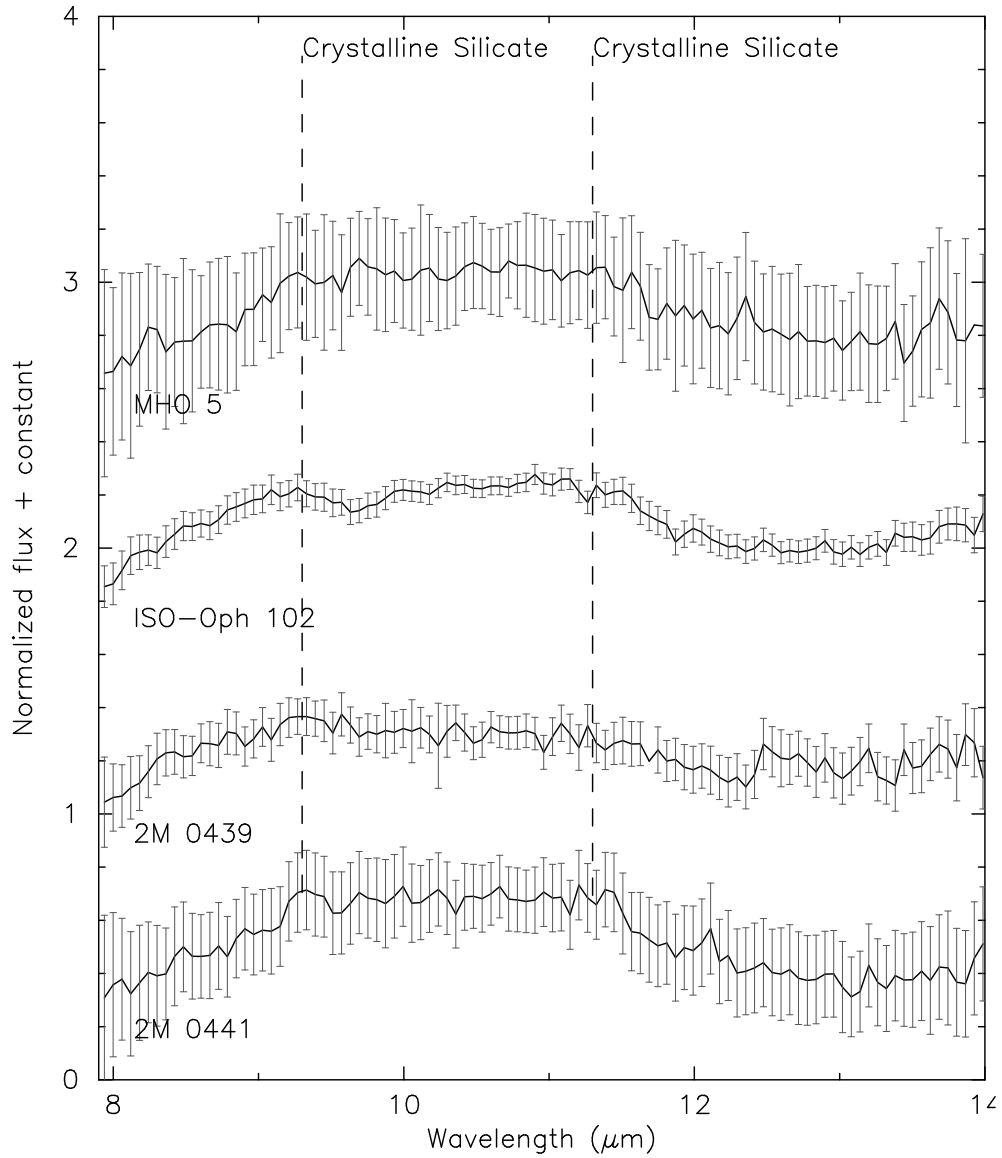


FIG. 3.— Spitzer infrared spectra of MHO 5, ISO-Oph 102, 2M 0439 and 2M 0441. Continuum subtraction was done following the literature (van Boekel et al. 2003; Apai et al. 2005). The crystalline silicate features at 9.3 mm (mainly enstatite) and 11.3 mm (forsterite) are indicated.

TABLE 1
OBSERVING LOGS FOR THE 4 YOUNG BDS AND VLM STARS

Target	Array	Configuration	Beam size ($" \times "$)	Region
MHO 5	SMA	Compact	3.05×2.82	Taurus
2M 0439	CARMA	D	2.60×2.48	Taurus
2M 0441	CARMA	D	2.02×1.86	Taurus
ISO-Oph 32	SMA	Compact	3.78×3.38	ρ Ophiuchi

TABLE 2
 ACCRETION AND MASS LOSS RATES FROM MHO 5 (TAURUS) AND ISO-OPH 102 (ρ OPHIUCHI), AND
 THE MASS LOSS RATE FROM THE EMBEDDED PROTO-BD CANDIDATE L1014-IRS

Target	Mass (M_J)	$\log(\dot{M}_{acc})$	$\log(\dot{M}_{out})$	References ^a
ISO-Oph 102	60	-8.9	-8.9	Natta et al. (2004); Phan-Bao et al. (2008)
MHO 5	90	-10.8	-9.1	Muzerolle et al. (2003); this paper
L1014-IRS			-8.7	Bourke et al. (2005)

^a References for accretion and mass loss rates